Differences in the Microrheology of Human Embryonic Stem Cells and Human Induced Pluripotent Stem Cells

Brian R. Daniels,[†△] Christopher M. Hale,[†‡△] Shyam B. Khatau,[†‡] Sravanti Kusuma,[†‡§] Terrence M. Dobrowsky,[†‡] Sharon Gerecht,[†‡] and Denis Wirtz[†‡*]

[†]Department of Chemical and Biomolecular Engineering, [‡]Johns Hopkins Physical Sciences in Oncology Center, and [§]Department of Biomedical Engineering, The Johns Hopkins University, Baltimore, Maryland

ABSTRACT Embryonic and adult fibroblasts can be returned to pluripotency by the expression of reprogramming genes. Multiple lines of evidence suggest that these human induced pluripotent stem (hiPS) cells and human embryonic stem (hES) cells are behaviorally, karyotypically, and morphologically similar. Here we sought to determine whether the physical properties of hiPS cells, including their micromechanical properties, are different from those of hES cells. To this end, we use the method of particle tracking microrheology to compare the viscoelastic properties of the cytoplasm of hES cells, hiPS cells, and the terminally differentiated parental human fibroblasts from which our hiPS cells are derived. Our results indicate that although the cytoplasm of parental fibroblasts is both viscous and elastic, the cytoplasm of hiPS cells does not exhibit any measurable elasticity and is purely viscous over a wide range of timescales. The viscous phenotype of hiPS cells is recapitulated in parental cells with disassembled actin filament network. The cytoplasm of hES cells is predominantly viscous but contains subcellular regions that are also elastic. This study supports the hypothesis that intracellular elasticity correlates with the degree of cellular differentiation and reveals significant differences in the mechanical properties of hiPS cells and hES cells. Because mechanical stimuli have been shown to mediate the precise fate of differentiating stem cells, our results support the concept that stem cell "softness" is a key feature of force-mediated differentiation of stem cells and suggest there may be subtle functional differences between force-mediated differentiation of hiPS cells and hES cells.

INTRODUCTION

Embryonic and adult fibroblasts can be returned to pluripotency by the expression of various reprogramming genes, including *Oct3/4*, *Sox2*, *c-Myc*, and *Klf4* (1). Despite the fact that hiPS cells are not identical to hES cells by global protein expression and epigenetic profiling (2,3), multiple lines of evidence suggest that they are indeed behaviorally, karyotypically, and morphologically similar (1). In particular, human induced plenipotent stem (hiPS) cells feature most of the human embryonic stem (hES) cell marker genes and can form embryoid bodies and teratomas, which differentiate normally, featuring all three germ layers. Moreover, hiPS cells injected into blastocysts contribute to embryonic development. Recently, Yu et al. (4) described a method using human fibroblasts, demonstrating that this technique could be used to supply pluripotent cells—derived from the patient's own cells—for biomedical applications. However, whether the physical properties of hiPS cells and hES cells, namely their micromechanical properties, are different, is unknown.

Recent studies have revealed the importance of extracellular matrix micromechanics on the specification of cell fate and differentiation (5,6). However, little is known regarding whether differentiated and undifferentiated cells feature different intracellular mechanical properties. Recent microrheology studies in *Caenorhabditis elegans* embryos suggest that large intracellular elasticity may be a property of differentiated cells and that cytoplasmic elasticity is effectively negligible in undifferentiated precursor cells (7). Subsequent magnetic twisting cytometry studies similarly revealed a significant difference between the rheological properties of differentiated and undifferentiated cell types in two different cell lines (8), supporting the concept that undifferentiated cells are significantly softer than their differentiated counterparts.

Here, using ballistic intracellular nanorheology (BIN) (9), we test this hypothesis directly by comparing the intracellular rheology of a well-controlled pair of differentiated parental human fibroblasts and hiPS cells derived directly from these parental human fibroblasts (Fig. 1). We also directly compare the microrheological properties of these cells to those of hES cells. Our results indicate that the cytoplasm of undifferentiated hiPS cells behaves as a viscous liquid with no measurable elasticity, whereas the cytoplasm of parental fibroblasts from which they are derived has both elastic and viscous properties. The viscous phenotype of undifferentiated hiPS cells can be recapitulated by disrupting the microfilament network in parental human fibroblasts, suggesting that structural rigidity derived from the actin network is not characteristic of undifferentiated hiPS cells. In contrast, although the cytoplasm of hES cells is also predominantly viscous, unlike that of hiPS cells it contains subcellular regions that are also elastic. Disruption

Submitted April 14, 2010, and accepted for publication October 7, 2010.

△Brian R. Daniels and Christopher M. Hale contributed equally to this work.

*Correspondence: wirtz@jhu.edu

Editor: Jason M. Haugh.

0006-3495/10/12/3563/8 $2.00

doi: 10.1016/j.bpj.2010.10.007

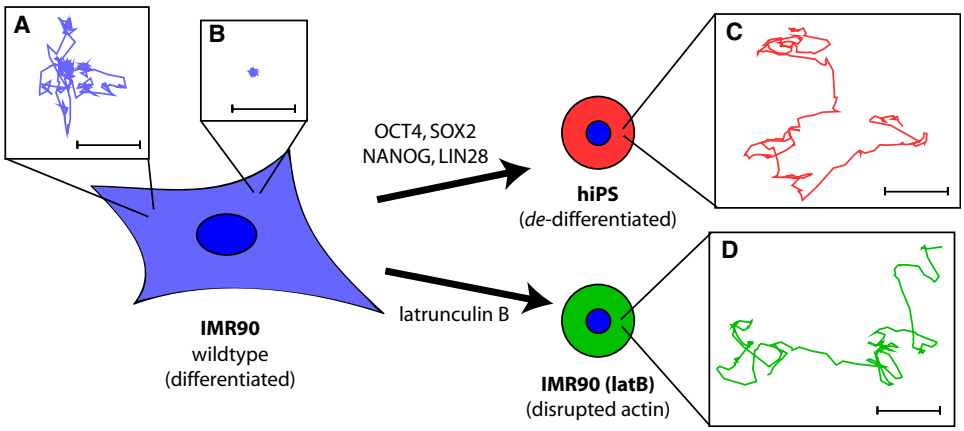

FIGURE 1 High-resolution trajectories of individual beads embedded in the cytoplasm of human parental fibroblasts, derived hiPS cells, and latB-treated fibroblasts. (*A* and *B*) Typical random displacements of 1.0-μm diameter beads embedded in the cytoplasm of parental IMR90 human fibroblasts can be either free-diffusing (*A*) or highly restricted (*B*). Typical displacements of beads embedded in the cytoplasm of (*C*) hiPS cells and (*D*) latB-treated IMR90 cells, which always undergo free diffusion. The centroid position of each bead was determined nine times per second for 22.2 s. Scale bars, 0.1 μm.

of the actin network in hES cells significantly decreased, but did not fully abrogate intracellular elasticity, suggesting that at least some of the elasticity observed in hES cells is not strictly due to the presence of actin filaments. Lower rigidity of the cytoskeleton network in undifferentiated hiPS cells and hES cells may contribute to their ability to readily respond to changes in the chemical and physical properties of the microenvironment (5,6).

EXPERIMENTAL PROCEDURES

Cell culture

Human IMR90 fetal lung fibroblasts (ATCC No. CCL-186; American Type Culture Collection, Manassas, VA) were cultured in DMEM supplemented with 10% bovine calf serum (American Type Culture Collection) and maintained at 37°C in a humidified, 5% CO_2 environment (10). hiPS cells were generated as described in Mali et al. (10) and generously offered by Prashant Mali and Linzhao Cheng (Johns Hopkins Medical School). After gene transduction, hiPS cells were cultured with standard hES cell medium (KO-DMEM, 20% KO Serum Replacement with 10 ng/mL bFGF) on irradiated feeders of mouse embryonic fibroblasts (10). hES were cultured in the same medium, but with 4 ng/mL bFGF. These cells were maintained at 37°C in a humidified, 5% CO_2 environment. Before Biolistic particle (BioRad, Richmond, CA) bombardment (see below), IMR90 cells were seeded at ~1 $\times$ 10^4 cells/mL on 35-mm cell culture dishes (Corning, Corning, NY), and hiPS and hES cells were transferred to a feeder-free culture on Matrigel (BD Biosciences, Franklin Lakes, NJ) coated plastic-bottom plates. After bombardment and recovery, all cell types were seeded at ~2 $\times$ 10^3 cells/mL on 35-mm glass bottom dishes coated with Matrigel (BD Biosciences). Cells were fixed immediately after tracking experiments for analysis by immunofluorescence microscopy.

Biolistic particle bombardment

The micromechanical properties of the cytoplasm were measured using BIN, as described previously in Lee et al. (11) and Panorchan et al. (12). A quantity of 1.0 μm-diameter fluorescent polystyrene beads (Invitrogen, Carlsbad, CA) was ballistically injected in the cytoplasm of cells using a Biolistic PDS-1000/HE particle delivery system (Bio-Rad). Beads were coated on macrocarriers, allowed to dry overnight before bombardment, and subsequently accelerated into the cytoplasm of cultured cells using 900-psi rupture disks in a 25 mmHg vacuum. Cells were washed repeatedly to eliminate free or physisorbed beads to mitigate endocytosis (which can lead to directed vesicular transport of beads within the cell) and allowed to recover overnight before imaging.

Multiple particle tracking microrheology

The motion of cytoplasmic fluorescent beads was recorded at nine frames per second for 200 frames using a Cascade 1K charge-coupled device camera (Roper Scientific, Tucson, AZ) mounted on a model No. TE2000E microscope with a 60$\times$ Plan Fluor lens (N.A. 1.4; Nikon, Melville, NY) controlled by Metavue software (Universal Imaging, West Chester, PA). In spread fibroblasts, we excluded beads from the cortical region, where the bounding membrane may appreciably hinder bead motion (which might lead to an overestimation of intracellular elasticity). Our analysis included all cytoplasmic beads from hiPS and hES cells. We typically tracked between one and four beads per cell, with the total number of beads indicated for each experimental setup (Fig. 2). Image acquisition and analysis were performed at 37°C and 5% CO_2. The two-dimensional trajectories of fluorescent beads embedded within the cytoplasm of living cells were determined using Metamorph software (Universal Imaging) and custom software designed to interpret particle motion (13). The intensity-weighted centroid of each bead was tracked with high spatial resolution (<5 nm) and used to determine individual two-dimensional time-averaged mean-square displacements (MSDs),

$$\langle \Delta r^2(\tau) \rangle = \langle [x(t+\tau) - x(t)]^2 + [y(t+\tau) - y(\tau)]^2 \rangle,$$

where τ is the time-lag and averaged over all possible times, t.

A cross-linked filamentous structure, such as a reconstituted F-actin network (14) or the cytoplasm (15,16), may have properties like a solid elastic gel or a liquid which can vary over a range of frequencies. Using a method similar to those previously described in Wirtz (9) and Mason et al. (14), the MSD profiles of the embedded beads were analyzed in terms of local viscous and elastic moduli of the cytoplasm. Viscosity, η, effectively describes the thickness of a liquid, or its propensity to flow and dissipate energy. The MSD of a particle in a viscous environment exhibits a linear relationship with time-lag (a slope of 1 on a log-log plot) through Einstein's relationship (9)

$$\langle \Delta r^2(\tau) \rangle = 4D\tau, \text{ or } \langle \Delta r^2(\omega) \rangle = \frac{4D}{\omega},$$

in terms of frequency, where τ is the time-lag, ω (= $1/\tau$) is the frequency, and D is the diffusion coefficient of the particle. The diffusion coefficient

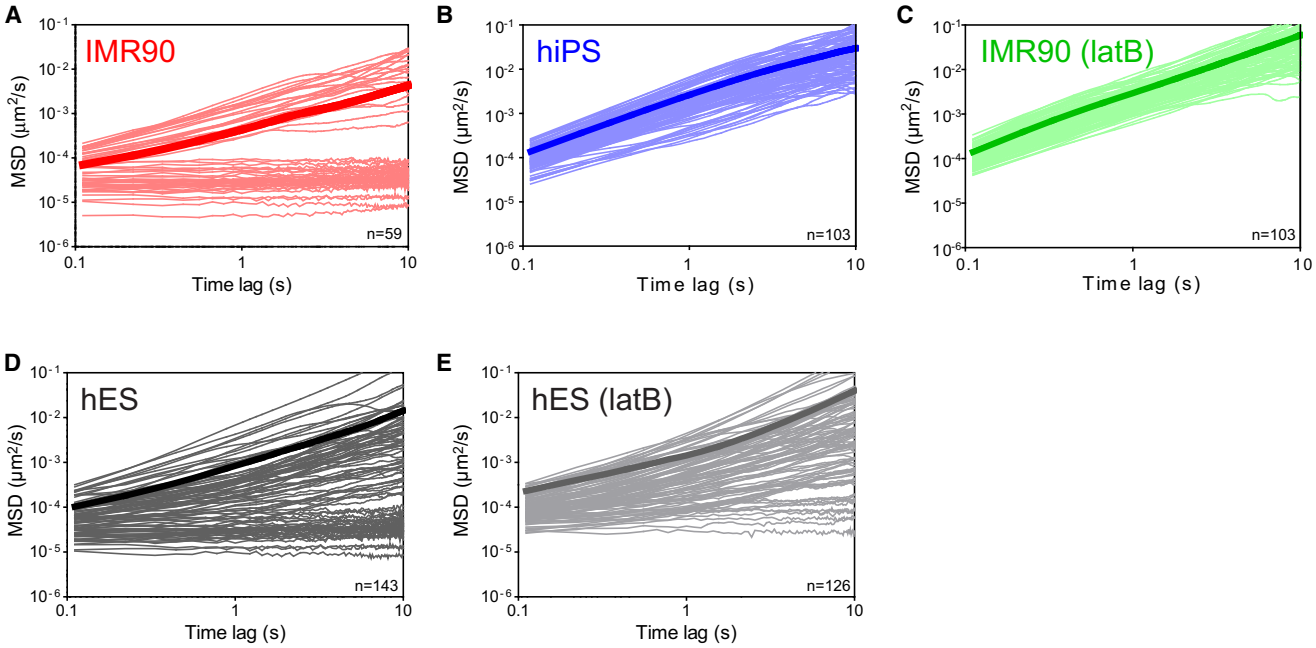

FIGURE 2 MSDs of beads in parental human fibroblasts, derived hiPS cells, and hES cells. (*A–E*) MSDs of individual beads embedded in the cytoplasm of parental IMR90 fibroblasts (*A*, $n = 59$), derived hiPS cells (*B*, $n = 103$), latB-treated IMR90 fibroblasts (*C*, $n = 103$), hES cells (*D*, $n = 143$), and latB-treated hES cells (*E*, $n = 126$). Time-lag-dependent MSDs exhibiting a slope <1 on a log-log plot (*A*, *D*, and *E*) are subdiffusive and indicative of a cytoplasm that is locally elastic, whereas slopes of 1 indicate a diffusive environment. Note the complete absence of subdiffusive MSDs in hiPS cells and the reduction of subdiffusive MSDs in latB-treated hES cells relative to untreated hES cells.

of a particle is inversely related to the viscosity through the Stokes-Einstein relationship (9)

$$D = \frac{k_B T}{6\pi\eta a},$$

where k_B is Boltzmann's constant, T is the absolute temperature, and a is the radius of the bead. Thus, the viscosity experienced by a nanoparticle undergoing viscous diffusion is related to the particle's MSD through the following equation:

$$\eta(\omega) = \frac{2k_B T}{3\pi a\omega\langle\Delta r^2(\omega)\rangle}.$$

The elastic modulus, G', describes the propensity of a complex fluid to store energy. Due to the fact that the motion of a bead in an elastic solid is effectively caged, its MSD exhibits a very weak dependence on time-lag (a slope of ~0 on a log-log plot). Briefly, the elastic modulus experienced by a nanoparticle embedded in an elastic medium is related to MSD using the following equation (14,17):

$$G'(\omega) = \frac{2k_B T}{3\pi a\langle\Delta r^2(\omega)\rangle}.$$

Local viscosity and elasticity can be inferred from the trajectory of an individual nanoparticle to survey spatial heterogeneity, or averaged to infer bulk viscoelastic properties. Because both the viscosity and elasticity measure the ability of a material to resist deformation, averaging the modulus of each bead (as opposed to using ensemble-averaged MSDs of all beads in a particular subset) has the advantage that small MSDs (high viscosity or elasticity) are not artificially obscured larger MSDs (lower viscosity or elasticity). Further details about the multiple-particle tracking method, including effects of various particle sizes and surface chemistry, have been presented previously in Wirtz (9) and Tseng et al. (13). We have chosen to represent quantities determined from the average values of individual particles with a bar ($\overline{\eta}$) and quantities determined from the ensemble-averaged MSD values with accents ($\langle\eta\rangle$).

Drug treatment

For F-actin disassembly experiments, IMR90 cells and hES cells were incubated in standard culture medium (see above) containing 1 μM latrunculin B (latB; Sigma, St. Louis, MO) for 30 min before and during particle tracking. Cells used in drug treatment experiments were exposed to latB for <2 h, and no change in rheology was detected during this time frame (data not shown). Cells were fixed immediately after particle-tracking experiments were completed.

Immunofluorescence microscopy

Cells were fixed with 3.7% formaldehyde for 30 min, washed with phosphate-buffered saline at room temperature, and permeabilized with 0.1% Triton X-100 for 10 min. Phosphate-buffered saline supplemented with bovine calf serum (10%) was used to block nonspecific binding, after which cells were treated with primary and secondary antibodies for 1 h each at room temperature. Actin and nuclear DNA were stained using Alexa Fluor 568 phalloidin (Invitrogen) at 1:40 dilution and 300 nM DAPI, respectively. The Tra-1-60 antibody (MAB4360; Chemicon, Temecula, CA) was used at 1:200 dilution. Cells were then cured in ProLong Gold antifade reagent (Sigma) and then covered with a coverslip before visualization. Fluorescent micrographs were collected using a Cascade 1K charge-coupled device camera (Roper Scientific) mounted on a model No. TE2000E microscope with a 60× Plan Fluor lens (N.A. 1.4; Nikon) controlled by Metavue (Universal Imaging).

Statistics

Mean values, standard error of measurement (mean ± SE), and statistical analysis were calculated using Microsoft Excel (Microsoft, Redmond, WA)

and plotted using Graphpad Prism (Graphpad Software, San Diego, CA). Two-tailed unpaired *t*-tests were conducted to determine significance between data sets. Significant differences are indicated as follows: *** for $p < 0.001$, ** for $p < 0.01$, and * for $p < 0.05$.

RESULTS AND DISCUSSION

For these studies, we chose well-characterized parental IMR90 human fetal lung fibroblasts and hiPS cells that were derived from these parental cells. hiPS cells were obtained through the expression of the reprogramming genes *Oct4*, *Sox2*, *NANOG*, and *LIN28* in IMR90 fibroblasts, while also adding a large SV40 antigen for improved efficiency and enhanced rate of cell generation, as described in Mali et al. (10). Because the biochemical properties and compliance of the substrate (18), as well as the composition of the culture medium (19) could influence the mechanical properties of cells, parental, hiPS, and hES cells were all grown in the same culture medium and seeded on the same matrigel-coated substrates. The micromechanical properties of the cytoplasm of these cells were probed using the recently introduced method of BIN (11,12).

Using ballistic bombardment to increase the efficiency of transfer of probing beads to the cells compared to manual injection (11), we introduced 1.0 μm-diameter polystyrene spherical beads into the cytoplasm of parental fibroblasts, hiPS cells, and hES cells. This bead size was chosen to be much larger than the effective mesh size of the cytoplasm of fibroblasts, which is ~50 nm (20). Ballistic injection of the probing beads directly into the cytoplasm, as opposed to their passive engulfment by the cells, circumvents the encapsulation of the beads inside endocytic/phagocytic vesicles (13), which would be actively transported toward the nucleus through motor proteins. After ballistic injection, overnight incubation allowed the beads to disperse throughout the cytoplasm.

We subsequently monitored the motion of the centroids of the fluorescent beads using high-magnification time-elapsed live-cell fluorescence microscopy to compute the time-averaged mean-squared displacement (MSD) of the beads,

$$\langle \Delta r^2(\tau) \rangle = \langle [x(t+\tau) - x(\tau)]^2 + [y(t+\tau) - y(\tau)]^2 \rangle,$$

where x and y are the time-dependent coordinates of the beads and τ is the time-lag (Fig. 2). We have recently demonstrated that the motion of beads lodged within the cytoplasm through direct injection is dominated by thermal Brownian forces and is not driven by activated by motor proteins, such as myosin II (21). Atypical MSDs displaying superdiffusive motion were excluded from analysis. We also verified that the movements of the beads were locally isotropic because the MSDs in the x and y directions had similar magnitude,

$$\langle \Delta x^2 \rangle \approx \langle \Delta y^2 \rangle$$

(not shown), precluding the need for three-dimensional tracking of the bead movements (see also (9)).

The MSDs of the beads embedded in the cytoplasm of IMR90 parental fibroblasts ($n = 59$), hiPS cells ($n = 103$), and hES cells ($n = 143$) were qualitatively and quantitatively different over a wide range of time-lags (Fig. 2). The MSDs of beads in hiPS cells showed exclusively diffusive behavior (Fig. 2 *B*) and were well described by Einstein's relationship

$$\langle \Delta r^2(\tau) \rangle = 4D\tau.$$

In contrast, the MSDs of beads embedded in the cytoplasm of parental fibroblasts featured two distinct subsets of beads (Fig. 2 *A*); one subset included beads that were freely diffusing, and the other subset included beads that were elastically trapped in the cytoplasm. Similar to beads in the cytoplasm of hiPS cells, the MSDs of the subset of freely diffusing beads in parental fibroblasts were also well described by the linear relationship $\langle \Delta r^2(\tau) \rangle = 4D\tau$. The elastic subset exhibited a negligible time-dependence over all probed time-lags ($\tau < 10$ s), and could be described by the relationship

$$\langle \Delta r^2(\tau) \rangle \approx \text{constant}.$$

The majority of the probing beads lodged in the cytoplasm of hES cells showed viscous diffusion; however, a small but significant fraction of these beads also showed elastic behavior with time-independent MSDs (Fig. 2 *D*).

Because the actin filament network provides most of the elasticity in somatic cells (19,22), we tested whether the purely viscous character of hiPS cells could be recapitulated by treating IMR90 parental fibroblasts with latrunculin B (latB), a drug that induces the disassembly of actin filaments by sequestering actin monomers and removing them from the polymerizable pool of actin. We found that latB treatment resulted in the complete loss of the elastic population of beads in parental fibroblasts, indicating that the elasticity experienced by the nanoparticles stems from the actin filament network and that the viscous phenotype of hiPS cells can be recapitulated by dismantling the actin filament network of IMR90 parental cells ($n = 103$, Fig. 2, *B* and *C*). The small fraction of beads displaying elastic behavior in hES cells was also reduced, but not completely eliminated, after treatment of hES cells with latB ($n = 126$, Fig. 2 *E*), suggesting the possibility that at least some of the elasticity seen in hES cells is not directly related to the actin cytoskeletal rigidity within the cells.

Further analysis of the distributions of MSDs in each cell type indicated a disproportionately large subpopulation (63%) of beads in the fibroblasts that exhibited restricted motion (Fig. 2 *A* and Fig. 3, *A* and *G*). The majority of the beads in the fibroblasts resided in the lowest bin in MSD histograms at both one-second and five-second time-lags

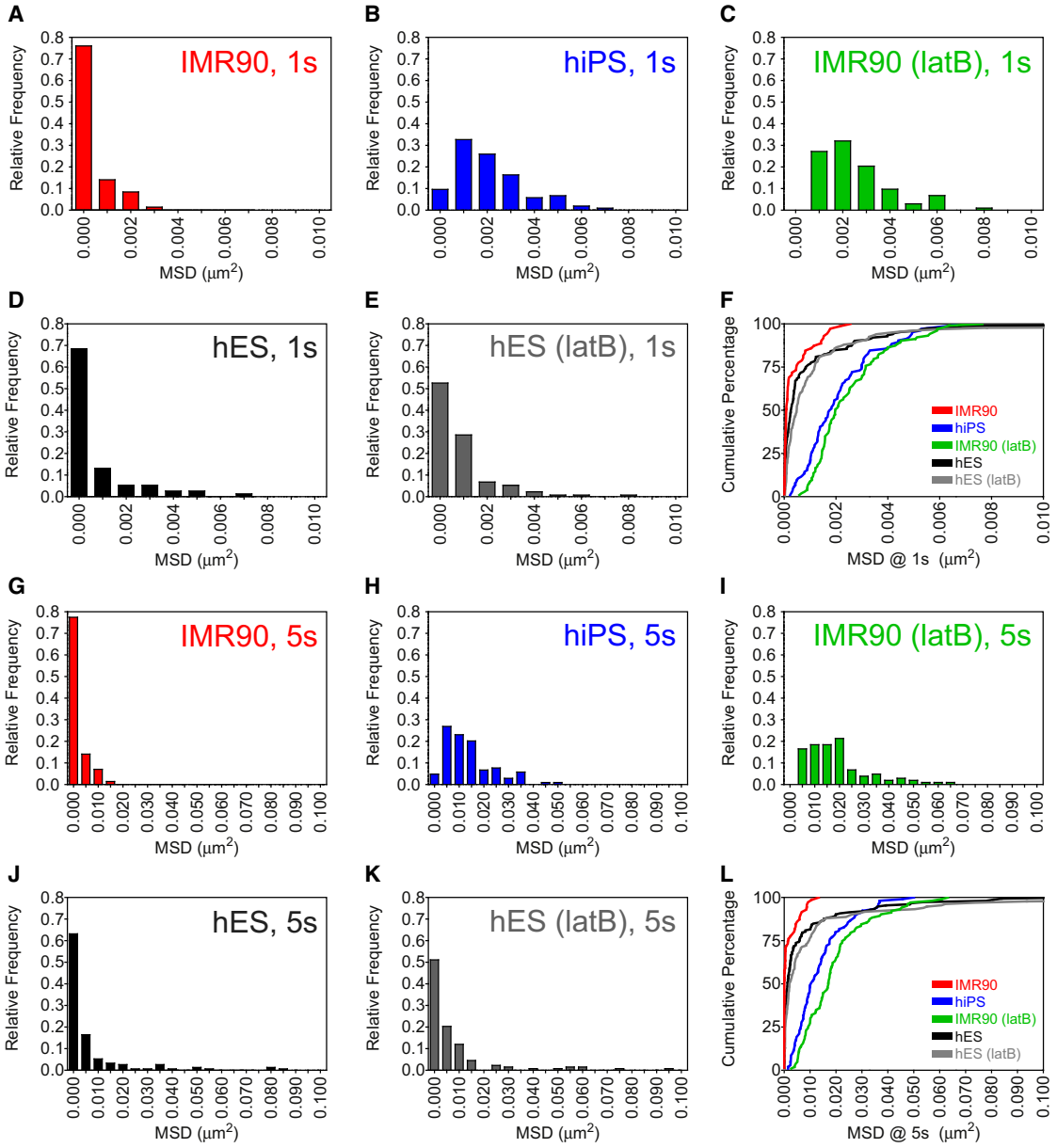

FIGURE 3 Beads exhibit restricted motion in parental human fibroblasts and hES cells. (*A–L*) Distributions of MSD values at both 1-s (*A–E*) and 5-s (*G–K*) time-lags of beads embedded in the cytoplasm of IMR90 fibroblasts (*A* and *G*), derived hiPS cells (*B* and *H*), latB-treated IMR90 fibroblasts (*C* and *I*), hES cells (*D* and *J*), and latB-treated hES cells (*E* and *K*). Histograms of these distributions indicate a disproportionately high number of small MSDs in IMR90 cells compared to hiPS at both 1-s and 5-s time-lags, as well as a larger number of small MSDs in hES cells compared to hES cells treated with latB at both time-lags. Cumulative percentage plots (*F* and *L*) indicate the percentage of beads that fall within a specified limit MSD. A disproportionate majority of beads in IMR90 differentiated cells exhibit restricted motion as compared to beads in hiPS de-differentiated cells.

(Fig. 3, *A* and *G*). In contrast, both hiPS cells (Fig. 3, *B* and *H*) and latB-treated fibroblasts (Fig. 3, *C* and *I*) exhibited distributions that were similar to those observed in early *C. elegans* embryos (7), i.e., the range of MSD values was narrow. Cumulative distribution plots revealed that a relatively small portion of beads in the fibroblasts underwent significant motion, and therefore disproportionally contributed to the ensemble-averaged MSD (Fig. 3, *F* and *L*). In contrast, beads in hiPS cells and latB-treated fibroblasts showed much more even contributions to the ensemble-averaged MSD (Fig. 3, *D* and *H*). The displacements of beads in the cytoplasm of hES cells showed an intermediate cumulative distribution at all tested timescales (Fig. 3, *F* and *L*), with only 26% displaying subdiffusive motion. Treatment of hES cells with latB did not significantly alter these distributions because of the prominence of viscous beads (Fig. 3, *D*, *E*, *J*, and *K*). These results indicate that fibroblasts featured a wide range of mechanical properties, whereas hiPS cells and latB-treated fibroblasts both showed a narrow range of cytoplasmic viscosity.

To calculate the mean diffusion coefficients of the freely diffuse beads in each cell type, we utilized the equation describing the Brownian motion of a bead in two dimensions, $\langle \Delta r^2(\tau) \rangle = 4D\tau$, where D is the diffusion coefficient and τ is the time-lag over which beads undergo random displacements. This linear relationship between MSD and time-lag indeed provided an excellent fit to the data ($R^2 > 0.98$ for all ensemble-averaged viscous data sets). We determined the average diffusion coefficients, D, up to a time-lag of 1 s for the beads in fibroblasts, hiPS cells, latB-treated fibroblasts, hES cells, and latB-treated hES cells to be 0.00028 ± 0.00003 $\mu m^2/s$, 0.00054 ± 0.00004 $\mu m^2/s$, 0.00063 ± 0.00004 $\mu m^2/s$, 0.00028 ± 0.00004 $\mu m^2/s$, and 0.00022 ± 0.00002 $\mu m^2/s$, respectively (mean $\pm$ SE; Fig. 4 *B*). For comparison, the diffusion coefficients of the same beads in water (viscosity, 0.01 Poise) and glycerol (viscosity, 1 Poise) are 0.4 $\mu m^2/s$ and 0.004 $\mu m^2/s$, respectively. We related the diffusion coefficients of the beads to the cytoplasmic viscosity probed by each bead using the Stokes-Einstein equation (9)

$$D = \frac{k_B T}{6\pi\eta a},$$

where k_B is Boltzmann's constant, T is the absolute temperature ($T = 310.15$K), a is the radius of the bead ($a = 500$ nm), and η is the shear viscosity of the milieu. We determined the mean shear viscosity at 1 Hz of parental fibroblasts, hiPS cells, latB-treated fibroblasts, hES cells, and latB-treated hES cells to be $\eta_{IMR90} = 24 \pm 3$ Poise or ~2400 times the viscosity of water, $\eta_{iPS} = 15 \pm 1$ Poise, $\eta_{IMR90(latB)} = 10 \pm 1$ Poise, $\eta_{hES} = 70 \pm 10$ Poise, and $\eta_{hES(latB)} = 60 \pm 10$ Poise, respectively (mean $\pm$ SE; Fig. 4 *C*). These results indicate that the viscosity of hiPS cells is significantly smaller than that of differentiated parental cells. The cytoplasmic viscosity of hES cells was higher than that of hiPS cells (Fig. 4 *C*) and latB treatment had no significant effect on the viscosity of hES cells (Fig. 4 *C*).

Using a method similar to that described in detail in Wirtz (9) and Mason et al. (14), we determined the elasticity of parental fibroblasts and hES cells directly from particles' MSDs (see Experimental Procedures). Because fibroblasts and hES showed subsets of beads with subdiffusive behavior (Fig. 4 *A*), we determined elastic moduli from both the ensemble-averaged MSDs and from the subset of beads with time-independent MSDs. Using ensemble-averaged MSDs of all particles, the cytoplasmic elasticity of fibroblasts at 1 Hz was 5.5 ± 0.8 dyn/cm^2, whereas the elasticities of hiPS cells, latB-treated IMR90s, hES cells, and latB-treated hES cells were negligible (data not shown). Using subdiffusive MSDs representative of elastic populations of particles, the cytoplasmic elasticity at 1 Hz of parental differentiated cells was determined to be 800 ± 100 dyne/cm^2 (mean $\pm$ SE; Fig. 4 *D*), which is similar in magnitude to the elasticity previously reported for other somatic cells and cultured human fibroblasts (7). In contrast, the elasticity of both hiPS cells and latB-treated IMR90 cells was negligible. These results indicate that the micromechanical character of the cytoplasm of hiPS cells and latB-treated IMR90 cells is the same: they are both highly viscous liquids, showing no hint of elasticity.

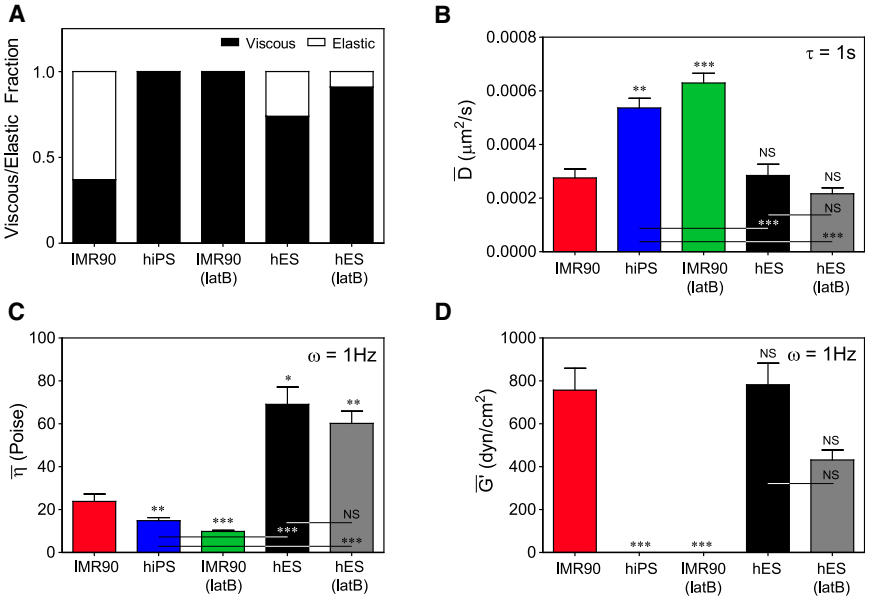

FIGURE 4 Diffusion coefficient of nanoparticles and viscosity of the cytoplasm of parental fibroblasts, derived hiPS cells, and hES cells. (*A*) Viscous and elastic fractions of particles observed in each condition. Particles were classified as viscous if their MSDs at a time-lag of 10 s were ≥ 0.000125 $\mu m^2/s$. (*B*) Mean diffusion coefficient, $\overline{D}$, of embedded beads. The MSDs of freely diffuse beads up to a time-lag of 1s were used to determine the bulk mean diffusion coefficient of beads in IMR90 and hiPS cells to be 0.00028 ± 0.00003 and 0.00054 ± 0.00004, $\mu m^2/s$, respectively. Asterisks or indications of no significance (NS) correspond to P values of t-tests between IMR90 values and each respective column. (*C*) Cytoplasmic viscosity is inversely related to the diffusion coefficient through the Stokes-Einstein relationship (see text). The mean viscosities, $\overline{\eta}$, of IMR90 and hiPS cells are 24 ± 3 and 15 ± 1 Poise, respectively ($P < 0.0001$). Asterisks or indications of NS correspond to P values of t-tests between IMR90 values and each respective column. (*D*) Mean elastic modulus, $\overline{G'}$, at 1 Hz calculated using only time-independent MSDs representative of elastic particles in each condition. Asterisks or indications of NS correspond to P values of t-tests between IMR90 values and each respective column.

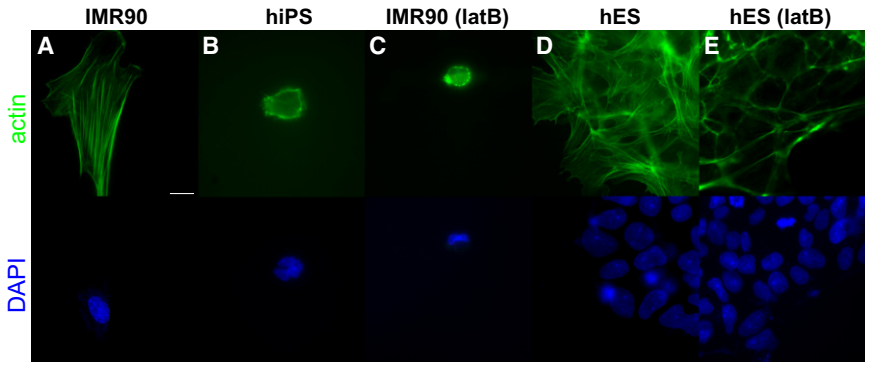

FIGURE 5 Actin microfilaments confer elasticity to differentiated parental fibroblasts and hES cells. (*A* and *B*) IMR90 fibroblasts and hiPS cells exhibit significantly different microfilament architecture. IMR90 cells contain a rich internal microfilament network typical of cultured fibroblasts, whereas hiPS cells are largely devoid of internal actin filament structure, such as filament bundles, reminiscent of the undifferentiated *C. elegans* zygote (7). (*C*) Depolymerization of actin filaments by latB in IMR90 cells led to a marked decrease in their elasticity down to values found for hiPS cells. (*D*) Colonies of hES cells show a rich basal actin microfilament structure, similar to that of IMR90 cells. (*E*) LatB treatment of hES cells largely depolymerized the intracellular actin network, whereas cortical actin structures remained intact. Scale bar, 20 μm.

Although viscous behavior dominated in hES and latB-treated hES cells (Fig. 4 *A*), small elastic populations were present, and thus their average cytoplasmic elasticities calculated from individual time-independent MSDs were nonzero and were 800 $\pm$ 100 dyne/cm^2 and 430 $\pm$ 50 dyne/cm^2, respectively. Treatment with latB not only reduced the elastic fraction in hES cells (from 26% to 9%) but also reduced the measured elasticity in these nonviscous subenvironments (Fig. 4). Thus, whereas a fraction of the nanoparticles in hES cells experienced intracellular elasticity similar in magnitude to that of parental fibroblasts, this elastic fraction of nanoparticles was much smaller in hES cells. Though hES cells typically contained only a single particle, the small elastic fraction of particles most likely represents elastic regions within hES cells, as opposed to an elastic population of differentiated cells within the hES population, because all tracked hES cells were Tra-positive (data not shown). The frequency responses of all measured elastic moduli were relatively constant for all frequencies (see Fig. S1 in the Supporting Material).

The predominance of the viscous character for the cytoplasm of hiPS cells contrasts with the predominance of an elastic character for the cytoplasm of parental IMR90 fibroblasts (Fig. 4) and that of all previously reported differentiated cells, including endothelial cells, epithelial cells, and other types of fibroblasts (9). Similar to previous studies in *C. elegans* embryos (23), immunofluorescence microscopy revealed that the actin cytoskeleton in hiPS cells existed predominantly as a meshwork of fine fibers and foci about the cortex, leaving the internal cytoplasm largely devoid of distinct actin structures (Fig. 5). Moreover, treatment of IMR90 cells with the actin-depolymerizing drug latrunculin B resulted in roughly spherical cells lacking obvious internal actin organization, evocative of the actin filament organization in hiPS cells (24,25). In contrast, hES cells showed a more extensive actin filament network than hiPS cells and, accordingly, showed partial elasticity.

These studies suggest that the onset of internal mechanical elasticity is a fundamental characteristic of differentiated cells and that the cytoplasm of hiPS cells is predominantly viscous over a wide range of timescales. Together, these findings strongly support the intriguing idea that changes in cytoplasmic viscoelasticity of a cell may correlate with its degree of differentiation (7), and support the recent finding that stem cell softness might be a key feature of force-mediated differentiation of stem cells (26). Finally, these studies highlight small but significant differences in the micromechanical properties of hES and hiPS cells, which may lead to functional differences in vivo.

SUPPORTING MATERIAL

One figure is available at http://www.biophysj.org/biophysj/supplemental/S0006-3495(10)01255-5.

We acknowledge the generous gift of hiPS cells and parental fibroblasts from Prashant Mali and Linzhao Cheng (Johns Hopkins School of Medicine), and thank Donny Hanjaya Putra and Elaine Vo for help with cell culture.

This research was supported in part by the National Institutes of Health-National Cancer Institute grants No. U54 CA143868 (D.W., S.G.) and No. R21CA137686 (D.W.), the O'Conner Starter Scholar award (S.G.), and the March of Dimes (S.G.).

REFERENCES

1. Takahashi, K., and S. Yamanaka. 2006. Induction of pluripotent stem cells from mouse embryonic and adult fibroblast cultures by defined factors. *Cell.* 126:663–676.
2. Chin, M. H., M. J. Mason, …, W. E. Lowry. 2009. Induced pluripotent stem cells and embryonic stem cells are distinguished by gene expression signatures. *Cell Stem Cell.* 5:111–123.
3. Doi, A., I. H. Park, …, A. P. Feinberg. 2009. Differential methylation of tissue- and cancer-specific CpG island shores distinguishes human induced pluripotent stem cells, embryonic stem cells and fibroblasts. *Nat. Genet.* 41:1350–1353.
4. Yu, J., M. A. Vodyanik, …, J. A. Thomson. 2007. Induced pluripotent stem cell lines derived from human somatic cells. *Science.* 318:1917–1920.
5. Engler, A. J., S. Sen, …, D. E. Discher. 2006. Matrix elasticity directs stem cell lineage specification. *Cell.* 126:677–689.

6. Even-Ram, S., V. Artym, and K. M. Yamada. 2006. Matrix control of stem cell fate. *Cell.* 126:645–647.
7. Daniels, B. R., B. C. Masi, and D. Wirtz. 2006. Probing single-cell micromechanics in vivo: the microrheology of *C. elegans* developing embryos. *Biophys. J.* 90:4712–4719.
8. Chowdhury, F., S. Na, …, N. Wang. 2008. Is cell rheology governed by nonequilibrium-to-equilibrium transition of noncovalent bonds? *Biophys. J.* 95:5719–5727.
9. Wirtz, D. 2009. Particle-tracking microrheology of living cells: principles and applications. *Annu. Rev. Biophys.* 38:301–326.
10. Mali, P., Z. Ye, …, L. Cheng. 2008. Improved efficiency and pace of generating induced pluripotent stem cells from human adult and fetal fibroblasts. *Stem Cells.* 26:1998–2005.
11. Lee, J. S., P. Panorchan, …, D. Wirtz. 2006. Ballistic intracellular nanorheology reveals ROCK-hard cytoplasmic stiffening response to fluid flow. *J. Cell Sci.* 119:1760–1768.
12. Panorchan, P., J. S. Lee, …, D. Wirtz. 2007. Probing cellular mechanical responses to stimuli using ballistic intracellular nanorheology. *Methods Cell Biol.* 83:115–140.
13. Tseng, Y., T. P. Kole, and D. Wirtz. 2002. Micromechanical mapping of live cells by multiple-particle-tracking microrheology. *Biophys. J.* 83:3162–3176.
14. Mason, T. G., K. Ganesan, …, S. C. Kuo. 1997. Particle tracking microrheology of complex fluids. *Phys. Rev. Lett.* 79:3282–3285.
15. Kole, T. P., Y. Tseng, and D. Wirtz. 2004. Intracellular microrheology as a tool for the measurement of the local mechanical properties of live cells. *Methods Cell Biol.* 78:45–64.
16. Tseng, Y., K. M. An, …, D. Wirtz. 2004. The bimodal role of filamin in controlling the architecture and mechanics of F-actin networks. *J. Biol. Chem.* 279:1819–1826.
17. Mason, T. G., and D. A. Weitz. 1995. Optical measurements of frequency-dependent linear viscoelastic moduli of complex fluids. *Phys. Rev. Lett.* 74:1250–1253.
18. Solon, J., I. Levental, …, P. A. Janmey. 2007. Fibroblast adaptation and stiffness matching to soft elastic substrates. *Biophys. J.* 93:4453–4461.
19. Kole, T. P., Y. Tseng, …, D. Wirtz. 2004. Rho kinase regulates the intracellular micromechanical response of adherent cells to rho activation. *Mol. Biol. Cell.* 15:3475–3484.
20. Luby-Phelps, K., P. E. Castle, …, F. Lanni. 1987. Hindered diffusion of inert tracer particles in the cytoplasm of mouse 3T3 cells. *Proc. Natl. Acad. Sci. USA.* 84:4910–4913.
21. Hale, C. M., S. X. Sun, and D. Wirtz. 2009. Resolving the role of actomyosin contractility in cell microrheology. *PLoS ONE.* 4:e7054.
22. Kole, T. P., Y. Tseng, …, D. Wirtz. 2005. Intracellular mechanics of migrating fibroblasts. *Mol. Biol. Cell.* 16:328–338.
23. Strome, S. 1986. Fluorescence visualization of the distribution of microfilaments in gonads and early embryos of the nematode *Caenorhabditis elegans*. *J. Cell Biol.* 103:2241–2252.
24. Gerecht, S., J. A. Burdick, …, G. Vunjak-Novakovic. 2007. Hyaluronic acid hydrogel for controlled self-renewal and differentiation of human embryonic stem cells. *Proc. Natl. Acad. Sci. USA.* 104:11298–11303.
25. Gerecht, S., C. J. Bettinger, …, R. Langer. 2007. The effect of actin disrupting agents on contact guidance of human embryonic stem cells. *Biomaterials.* 28:4068–4077.
26. Chowdhury, F., S. Na, …, N. Wang. 2010. Material properties of the cell dictate stress-induced spreading and differentiation in embryonic stem cells. *Nat. Mater.* 9:82–88.